AN ENVIRONMENTAL IMPACT STUDY OF ORION NEBULA DUST

JASON A. CARDELLI[a] AND GEOFFREY C. CLAYTON
Washburn Observatory, University of Wisconsin-Madison, Madison, Wisconsin 53706
Received 1 September 1987; revised 13 October 1987

ABSTRACT

In this paper, new high-quality extinction curves are presented for θ^1 Ori A, C, and D, and θ^2 Ori A and B, over the wavelength range 3300–6000 Å. These are coupled with near-infrared and ultraviolet data to produce extinction curves from 0.12 to 3.5 μm. The Orion Nebula region is interesting in that most of the known processes of dust-grain growth, processing, and destruction may be operating nearly simultaneously in close proximity to one another. Each of these processes is considered with respect to the observed extinction curves and environmental conditions in the Orion Nebula and its associated molecular cloud. Plausible grain populations are fit to the observed extinction curves. A good fit to the average θ Ori extinction curve can be obtained with: (1) a combination of larger than normal silicate grains produced through coagulation and accretion; (2) evaporation of volatile mantles; (3) a reduction in the column density of small (<0.01 μm) grains responsible for the bump and far-ultraviolet extinction through differential acceleration due to radiation pressure, and possible evaporation. It seems plausible to explain the observed peculiar extinction in the Orion Nebula simply by environmental effects on otherwise normal grains.

I. INTRODUCTION

The study of interstellar dust in the Orion Nebula is over 50 yr old. The reddening of θ^1 Ori was first measured by photoelectric photometry with the 15.6 in. refractor at Washburn Observatory (Stebbins and Huffer 1934). The anomalous nature of the Orion dust was discovered shortly thereafter by Baade and Minkowski (1937). They found that the optical extinction curve of the Orion stars could be fit by using larger than normal grains and suggest that smaller grains would be preferentially removed by radiation pressure which has created a cavity in the nebula centered on the Trapezium. Since 1937, the nature of the Orion dust has been a source of controversy. But today, 50 yr later, the anomalous Orion extinction is still typically attributed to larger than normal grains whose size distribution may have been altered by radiation-pressure effects.

Several studies of visual and infrared colors of the Orion stars find large values of R, the ratio of total to selective extinction, indicating the presence of large grains (e.g., Anderson 1970). Johnson (1967) and Lee (1968) found that $R \approx 5$ in the central part of the Orion Nebula. On the other hand, Penston, Hunter, and O'Neill (1975) find that R is normal (≈ 3). More recently, Breger, Gehrz, and Hackwell (1981) calculated R and λ_{max}, the wavelength of maximum interstellar polarization, both considered to be grain-size parameters, for a large number of Orion stars. Both parameters are found to be large for lines of sight toward the nebular region but are normal for sight lines just outside of the nebulosity.

Recently, Clayton and Mathis (1988) suggested that extinction curves are largely invariant to the red of 7000 Å, with variations in R manifested at the blue end of the visual extinction curve. This fits in well with measurements of the ultraviolet (UV) extinction toward θ^1 Ori A, B, C, D, and θ^2 Ori A and B, which were found to be very anomalous (Bohlin and Savage 1981). The extinction curves are very different from the average Galactic curve, showing extinction from 3200 to 1200 Å, which is very much smaller than normal. The 2175 Å bump is present but is somewhat weaker than normal. Similarly anomalous extinctions were found for several other Orion Nebula lines of sight, including NU Ori and LP Ori, by Panek (1983). Similar but not as extreme UV extinction is seen for stars associated with the ρ Oph dark cloud (Wu, Gilra, and van Duinen 1980; Bohlin and Savage 1981; Massa, Savage, and Fitzpatrick 1983) and also in the innermost portion of the 30 Doradus nebula (Fitzpatrick and Savage 1984).

The environment of the Orion dust is one in which you would expect significant grain evolution to occur. McCall (1981) suggests several mechanisms for altering the grain-size distributions in a region such as the Orion Nebula. They include radiation pressure, which may separate small and large grains, and grain accretion, evaporation, and coagulation, which would alter the mean grain size. There is the molecular cloud complex in which grains would be expected to accrete or coagulate. The Trapezium stars, θ^1 Ori A, B, C, and D, are the youngest in a sequence of star formation that is eating into the background molecular cloud (Goudis 1982). The dust near the Trapezium is now in an H II region and is being subjected to intense UV radiation, stellar winds, and radiation pressure. Therefore, once outside the molecular cloud, dust grains may encounter a harsh environment.

In this paper, new extinction curves are presented for θ^1 Ori A, C, and D, and θ^2 Ori A and B, over the wavelength range 3300–6000 Å. When coupled with near-infrared (IR) and UV data, good-quality extinction curves from 0.12 to 3.5 μm can be produced. These new data present an opportunity to re-examine the characteristics of the Orion dust in the light of what is presently known about its environment.

II. OBSERVATIONS AND REDUCTIONS

The spectrophotometric data presented here were obtained on UT 3–7 October 1982 using the Intensified Reticon Scanner (IRS) on the KPNO No. 1 0.9 m telescope. The system consists of a cooled dual-beam multichannel Reticon coupled with the white spectrograph. The setup used consisted of grating No. 26 (600 lines/mm), which is blazed at 4000 Å. The data were obtained over the wavelength range 3300–6000 Å with a 13.5″ aperture, which corresponds to a resolution of ≈ 9.7 Å. Basic data for the program objects are listed in Table I. The V and $B-V$ data represent an average

[a] Guest Observer, KPNO, operated by AURA, Inc., under contract to the National Science Foundation.

 0004-6256/88/020516-10$00.90

TABLE I. Reddened and comparison stars.

HD	Name	V	B-V	Sp Type	E(B-V)	References
37020	θ^1 Ori A	6.72	0.02	O8 V-B0.5 Vp	0.30[a]	c,d,e,f,g
37022	θ^1 Ori C	5.13	0.01	O6ep-O7 V	0.31	c,d,e,f,h
37023	θ^1 Ori D	6.70	0.09	O9.5 V-B0.5p	0.35	e,f,g
37041	θ^2 Ori A	5.07	-0.10	O9 V-O9.5 Vp	0.19	c,d,e,f,g,h
37042	θ^2 Ori B	6.40	-0.11	B0.5 Vp-B1 V	0.17	e,f,g
47839	15 Mon	4.65	-0.25	O7 V-O 8 V	0.06[b]	c,d,h
36512		4.62	-0.27	B0 V	0.02	c,h,i,j
34816	λ Lep	4.29	-0.27	B0.5 IV-V	0.02	h,i
31726		6.15	-0.22	B1 V	0.04	h,i

(a) E(B-V) for θ Ori stars from extinction curve fit.

(b) E(B-V) for comparison stars from Johnson (1958), Garrison (1967), FitzGerald (1970).

(c) Johnson (1966)

(d) Conti and Aschuler (1971)

(e) Lee (1968)

(f) Carruthers (1969)

(g) Underhill (1966)

(h) Lesh (1968)

(i) Cousins, Lake, and Stoy (1966)

(j) Walborn (1971)

of the data found in the literature. In general, the dispersion about the average values is ± 0.02 for V and ± 0.01 for $B-V$.

A minimum of two standard stars from the IRS Standard Star Manual (reobserved Oke standards) were observed each night for the purpose of monitoring the atmospheric extinction and producing an accurate flux-calibration function. The standard stars were observed a number of times over a range of airmass of $1 \leqslant X \leqslant 2$. The atmospheric-extinction curve produced from these observations was within 10% of the standard KPNO site extinction for the entire wavelength range. Consequently, the well-established site-extinction curve was used. The program objects listed in Table I were observed over a fairly narrow range in airmass (± 0.2) roughly centered at $X = 1.4$. The purpose of this was to ensure that any possible systematic errors introduced in the extinction correction would be approximately the same for all of the observations including the IRS standard stars, which corresponded to about the same average airmass. Consequently, any systematic color variations present in the data through improper extinction correction should be largely removed in the flux calibration. The significance of this is discussed in Sec. III.

For the range of airmass discussed above, the final standard-star fluxes showed no apparent variation with wavelength when compared with their respective published fluxes for any of the nights. There was a slight zero-point shift in some of the observations, but this amounted to no more than a few percent. In addition, the reduced observations of each star from the four of the five nights that were photometric were compared to determine any night-to-night variations. Again, no noticeable color errors were seen, and the total zero-point spread in flux was of the order of a few percent, which is well within the uncertainty of the fluxing procedure itself.

For each object, all of the data have been summed for the four nights. Because the IRS apertures are separated by 1', the average 'sky' measurements for each star corresponded to positions of 1' east and west which included both nebular emission and scattered light from dust. This was considered desirable since our goal was to remove as much of the nebular contamination as possible. The emission lines visible in the spectrum of θ^1 Ori C correspond to residual nebular contamination from the λ 4959 and λ 5007 lines of [O III]. These lines are seen in absorption for the θ^2 Ori A and B spectra. Also, for the θ^1 Ori C data, the effect of residual hydrogen Balmer-line contamination can be seen in the Hβ, Hγ, and Hδ lines. The possible effects of residual nebular contamination on the derivation of the extinction curves is discussed in Sec. III below.

III. OPTICAL EXTINCTION CURVES

a) Derivation

The extinction curves presented here were derived using the standard-pair method. Briefly, this involves comparing the colors $m(\lambda - V)$ of the reddened program star with the

dereddened colors of a lightly reddened or unreddened comparison star. The derived curves are then normalized in the usual fashion (i.e., by $E(B-V)$).

It is evident from Table I that there is some uncertainty in the literature connected with the spectral types of the $\theta^{1,2}$ Ori stars. Consequently, the proper comparison stars were not chosen blindly based upon any particular published type but were based upon the strength of the hydrogen Balmer lines shortward of Hδ, the Balmer jump, and the temperature-sensitive lines of He I (λ 4144,4471,4922), He II (λ 4542,4686), and C III (λ 4647–51). As it turns out, the most serious effect related to spectral mismatch is the Balmer jump and so this was viewed as the most serious criterion for fixing the proper spectral type (see below). From the comparison-star data in Table I, all three of the above classification criteria yield the same mean range of spectral type (about half a spectral class), with the exception of θ^1 Ori D, for which the He lines yield O9.5 V–B0 V, while the Balmer jump indicates B0 V–B0.5 V. In addition, the ranges are consistent with the ones shown in Table I, with the exception of θ^2 Ori A, for which we find B0 V to be the most suitable comparison. Also, based on all the above criteria we find that O8 V is much too early for θ^1 Ori A and that B0 V is the earliest type for which a good match is found. We should note at this point that additional examples of spectral types O5 V–B1 V were obtained from the atlas of Jacoby, Hunter, and Christian (1984) in order to fill in some obvious gaps in the *classification* sequence but were *not* used to determine the final curves for two major reasons. First, most of their stars have $E(B-V) \geqslant 0.5$, which increases the probability of reddening-correction problems. Second, and most important, is the possibility of photometric mismatch between the two data sets, particularly for the region $\lambda < 4000$ Å. As described in Sec. II, the major reason all of the data in Table I were obtained at the same mean airmass was to reduce photometric errors as much as possible. Therefore, any systematic photometric errors in the calibrated flux should be essentially the same for all of our objects.

The derived normalized optical extinction curves for the θ Ori stars are shown in Figs. 1 and 2. The data were first smoothed over five points ($\approx$14 Å) in order to reduce the noise. The $E(B-V)$ values listed in Table I arise from the derived curves by defining $E(\lambda-V)/E(B-V) = 0$ and 1 at $V(\lambda_{\rm eff} = 5470$ Å) and $B(\lambda_{\rm eff} = 4400$ Å), respectively. In general, these values agree to better than 0.02 mag with $E(B-V)$ values listed by Bohlin and Savage (1981) and Johnson (1968) determined from broadband data. The residual contamination by nebular line emission can be seen shortward of $\lambda^{-1} = 2.5\,\mu{\rm m}^{-1}$ as 'absorption' and 'emission' spikes for the θ^1 Ori and θ^2 Ori curves, respectively. Also plotted are the near-IR extinction data of Johnson (1966), the near-UV portion of the UV curves of Bohlin and Savage (1981), and the relevant portion of the average interstellar extinction curve (UV: Seaton 1979; optical: Whitford 1958; Rieke and Lebofsky 1985).

As can be seen in the figures, the normalized optical portions of the curves match very well with the near-UV and IR portions. The error bar in each figure represents the magnitude variation in extinction that would result from a *relative* flux error of 10% for the respective mean reddening of the θ^1 and θ^2 Ori directions. With one exception (λ Lep), no common comparison stars were used in fitting the three segments together. Instead, the data were taken from their respective sources as is. However, in order to be consistent, the UV and IR data have been renormalized to the $E(B-V)$ values listed in Table I. Although inconsistent use of comparison stars can affect the overall shape of the normalized IR and UV segments, the effect in the overlap regions shown in Figs. 1 and 2 will be negligible, especially considering the general agreement in spectral types used to determine the three segments (see discussion below). For the θ^1 Ori C UV curve, Bohlin and Savage used an O9.5 IV comparison star which, compared to an O6 V, exhibits a Balmer jump that is about 7% stronger. Consequently, a shift of + 0.25 mag has been added to the UV curve.

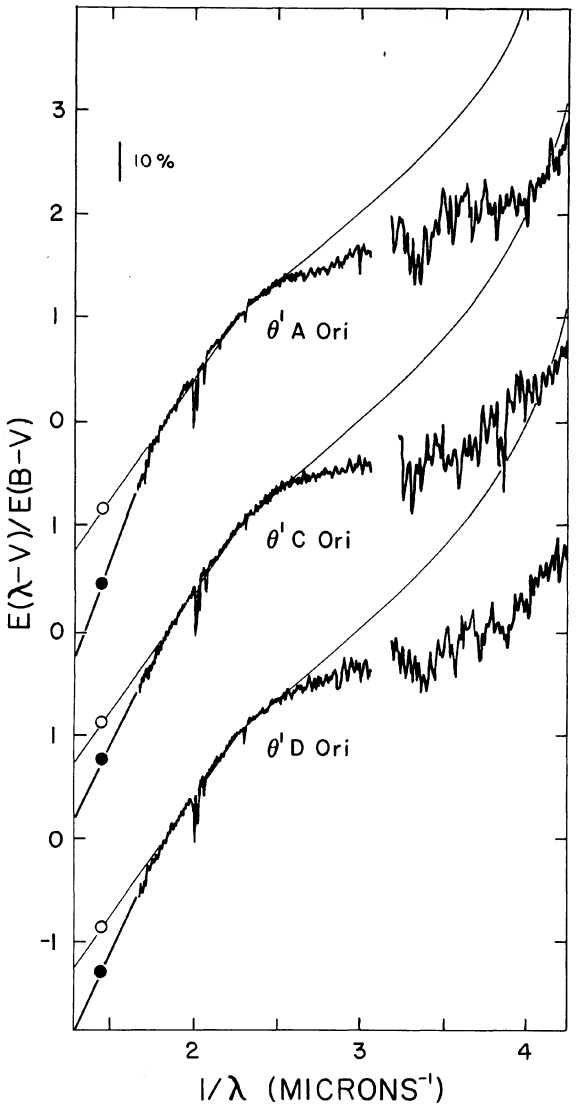

FIG. 1. Optical extinction curves derived from the observations of the θ^1 Ori stars. The thin curve represents the average interstellar extinction curve and was taken from Seaton (1979), Whitford (1958), and Rieke and Lebofsky (1985; light circles). The near-UV data were taken from Bohlin and Savage (1981), while the near-IR data are from Johnson (1966; dark circles). The error bar corresponds to the extinction error that could be expected from a relative flux error of 10%. Note how well the three independent segments fit together.

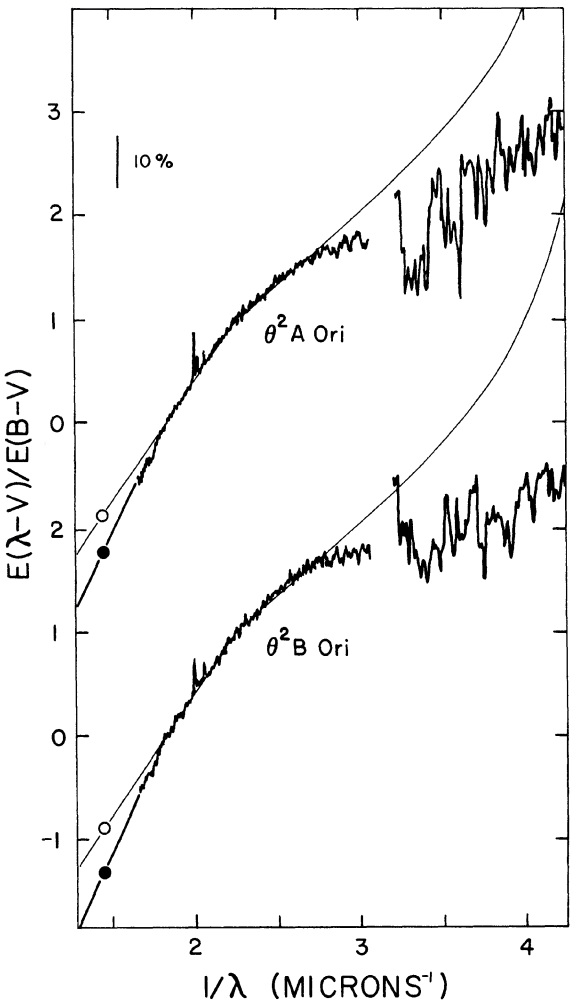

FIG. 2. Optical extinction curves derived from the observations of the θ^2 Ori stars. Everything else is the same as in Fig. 1. Again, note how well the three independent segments fit together.

b) Sources of Error

In order to appreciate fully the accuracy of the curves shown in Figs. 1 and 2, one must consider all possible sources of uncertainty, both random and systematic. A complete discussion of the sources and magnitude of such errors for derived extinction curves can be found in Massa, Savage, and Fitzpatrick (1983) and Massa and Fitzpatrick (1986). Although these references specifically discuss UV curves derived from *IUE* data, the general principles can be applied to any derived curve. For our extinction curves, the sources of random error, in principle, include uncertainty in the zero-point photometric calibration and the values ΔV and $E(B-V)$ used to normalized the curves. However, because these are optical curves and are defined by requiring $\langle E(\lambda-V)/E(B-V)\rangle = 0$ and 1 at V and B, respectively, uncertainties in $E(B-V)$ are not independent of the general wavelength-dependent photometric errors and so random errors will result from the zero-point photometric-calibration errors only. As discussed in Sec. II, the apparent zero-point errors of a few percent are not applicable because they are removed in the normalization process. Consequently, random errors in our curves are negligible.

The major sources of possible systematic errors in our derived curves include wavelength-dependent photometric-calibration uncertainty, temperature (spectral type) mismatch, improper dereddening of the comparison star, and contamination of the θ Ori observations by nebular emission and scattered light.

As discussed in Sec. II, the calibrated data show no apparent wavelength-dependent uncertainty down to 1% over the entire observed wavelength range. For the normalized curves in Figs. 1 and 2, this translates to relative flux errors of less than 1% and hence extinction errors of less than 0.02 mag. Again, these relative errors are small because all of the program objects were observed and reduced at about the same mean airmass.

As discussed in Sec. III*a*, great care was taken to properly match the program and comparison stars, particularly at the Balmer jump. It turns out that over the narrow range of applicable spectral types for each star, the shapes of the normalized curves are invariant to mismatch errors from 1.7 $\mu m^{-1} \leqslant \lambda^{-1} \leqslant 2.6\,\mu m^{-1}$. The exception to this is the Balmer jump. Mismatch of ± 1 spectral class at B0 V results in a shift of the segment of the curve above $\lambda^{-1} = 2.6\,\mu m^{-1}$ by about ± 0.12 and 0.18 for $E(B-V) = 0.3$ and 0.2, respectively. However, because the Balmer jump is rather discrete, such a mismatch can be easily seen. In addition, mismatch of the Balmer lines longward of the jump is also visible. For our program stars, the Balmer jumps have been matched to a relative accuracy of $\leqslant \pm 0.005$ in $\Delta \log F_\lambda$ as measured from above and below the Balmer jump which corresponds to a relative extinction error of $\leqslant \pm 0.04$ mag for θ^1 Ori curves and $\leqslant \pm 0.06$ for θ^2 Ori curves. It is important to note that the *slope* of the segment above $\lambda^{-1} = 2.6\,\mu m^{-1}$ is invariant to mismatch at the Balmer jump. Thus, while the zero-point position of the curve above $\lambda^{-1} = 2.6\,\mu m^{-1}$ has the above uncertainties associated with it, the general shape of the curves is unchanged.

From the convention of Massa, Savage, and Fitzpatrick (1983), the errors introduced through improper dereddening of the comparison star have the form $[E(B-V)_c/E(B-V)] \times [k(\lambda-V)_c - k(\lambda-V)]$, where $E(B-V)_c$ and $E(B-V)$ are the color excesses of the comparison and program star, respectively, $k(\lambda-V)_c$ is the normalized extinction curve appropriate for the comparison star, and $k(\lambda-V)$ is the assumed average extinction curve. Given the general observed invariance of normalized optical extinction curves, it is unlikely that the proper normalized extinction curves for the comparison stars differ by more than 0.1 mag relative to the average curve. For the most extreme case (i.e., $E(B-V)_c = 0.06$, $E(B-V) = 0.17$, and $\Delta k(\lambda-V) = 0.1$), the relative error is only ± 0.04 mag. For our data, the applicable error is a factor 2–3 less than this value. Another possible related error is the effect introduced in the comparison-star reddening correction by the uncertainty in $E(B-V)_c$. Assuming $\Delta E(B-V)_c = \pm 0.015$ mag, this error amounts to no more than ± 0.01 mag.

Possible contamination of the data of $\theta^{1,2}$ Ori by nebular emission and scattered light is probably the worst systematic error affecting our data since one can expect that the resulting effects on the extinction curves would mimic exactly the abnormal behavior that is observed. Despite the fact that the sky measurements were made within 1′ east and west of each

star, the residual effects of nebular line emission are still present. In order to examine possible residual continuum contamination, we have utilized an analysis of the spatial dependence of nebular emission in the Orion Nebula in the UV (Mathis *et al.* 1981) and optical (Schiffer and Mathis 1974).

From Mathis *et al.* (1981) we find that for a distance of 1′ from θ^1 Ori C the average surface brightness of the nebula (nebular emission plus scattering), I_λ, is about 1.4×10^{-4} erg cm^{-2} s^{-1} Å^{-1} sr^{-1} at 3000 Å, with about 60% of the contribution coming from scattering. For our entrance aperture, this corresponds to a total nebular flux f_λ of about 6×10^{-13} erg cm^{-2} s^{-1} Å^{-1}. From the data and model results of Schiffer and Mathis (1974) and Mathis *et al.* (1981) we find that the total flux contribution at the position of θ^1 Ori C is no more than $f_\lambda = 1.4\times10^{-12}$ erg cm^{-2} s^{-1} Å^{-1}, yielding a ratio of nebular to stellar flux at 3000 Å of $f_{3000}/F_{3000}\leqslant6\times10^{-3}$ or 0.6%. At 3646 Å, just shortward of the Balmer jump, the contribution of scattered light has decreased by about 30%, while the contribution from nebular hydrogen Balmer continuum emission has peaked at a value about twice its value at 3000 Å (Osterbrock 1974). From this, we find $f_{3646}/F_{3646}\leqslant1\times10^{-2}$, or 1%. Immediately longward of the Balmer jump, the ratio has dropped to about 5×10^{-3} and continues to decrease ($f_{4500}/F_{4500}\leqslant3\times10^{-3}$). Accounting for the fact that the sky measurements were obtained 1′ east/west of θ^1 Ori C, the actual contribution is about 30%–50% less. Consequently, the effect of nebular contamination on the normalized optical extinction curve for θ^1 Ori C is less than 0.02 mag. It is interesting to note that the most serious effect of this contamination will be to add a near zero-point shift in the segment of the curve above $\lambda^{-1} = 2.6\,\mu\text{m}^{-1}$ which mimics the effect created by a mismatch at the Balmer jump.

Because they are fainter than θ^1 Ori C, the amount of contamination for θ^1 Ori A and D, if dominated by the effects of θ^1 Ori C, could be as much as 2–3 times greater. However, Fig. 1 shows no significant difference between any of the θ^1 Ori extinction curves and so the contamination is probably no more than 1%. Finally, because the nebula is much fainter towards θ^2 Ori A and B, we feel that nebular contamination is negligible.

Collecting the errors together and noting that their contributions are independent of each other, we find the overall error in the computed extinction curves for $\lambda^{-1}\leqslant2.6\,\mu\text{m}^{-1}$ to be less than $\pm$ 0.03 mag for both θ^1 and θ^2 Ori. For $\lambda^{-1}>2.6\,\mu\text{m}^{-1}$, the uncertainty is dominated by a zero-point error of $\leqslant\pm$ 0.04 mag and 0.06 mag for the θ^1 Ori and θ^2 Ori curves, respectively.

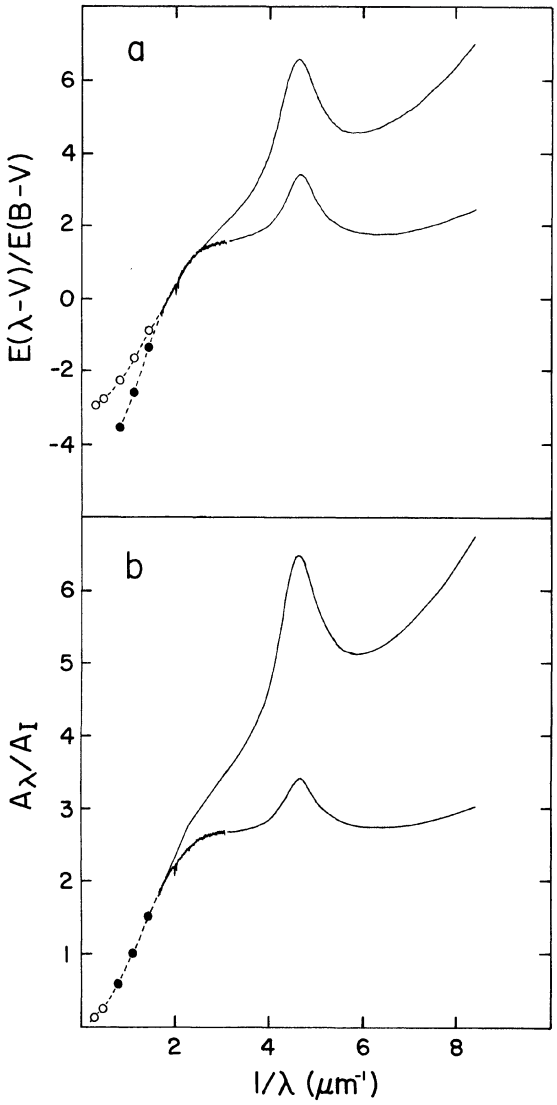

FIG. 3. The average extinction curve for θ Ori (dark circles, lower UV curve) compared to the average interstellar curve. The sources for the data represented by light and dark circles are the same as in Fig. 1. (a) The extinction curves are normalized at $E(B-V)$. Data for the K and L passbands have not been included for the θ Ori curve because they appear contaminated by emission. (b) The absolute extinction curves normalized at the I passband. The fit for the θ Ori curve corresponds to $A_v/E(B-V)\approx5$.

IV. DISCUSSION

a) Comparison with Other Extinction Curves

1) Optical and infrared

Examination of Figs. 1 and 2 reveals a well-known and important shortcoming associated with the normalization of extinction curves in the optical region. For the most part, the only place where the θ Ori curves match the average curve is at the normalization points. The magnitude of the deviations is even more impressive when the entire observed extinction curve ($0\,\mu\text{m}^{-1}<\lambda^{-1}<9\,\mu\text{m}^{-1}$) is displayed as in Fig. 3(a). The extinction data for θ Ori at the $K(2.2\,\mu\text{m})$ and L ($3.4\,\mu\text{m}$) passbands clearly show the effects of near-IR emission contamination (Johnson 1966) and have not been plotted. In order to understand fully exactly how much and where the θ Ori curve deviates from the norm, a normalization must be chosen such that places where real changes in the shape of the extinction curve are avoided.

Figure 3(b) displays the same data as in Fig. 3(a), except scaled by $R[A_v/E(B-V)]$ and normalized at $I(\lambda=0.90\,\mu\text{m})$. For the average interstellar curve, the data of Rieke and Lebofsky (1985) have been used with $R = 3.1$. For θ Ori, we initially used the value $R\approx5$ from Johnson (1968), which was derived by extrapolating the curve from the region $0.8\,\mu\text{m}^{-1}\leqslant\lambda^{-1}\leqslant1.43\,\mu\text{m}^{-1}$. Admittedly, this is somewhat circular, since one must assume a curvature for $\lambda^{-1}\leqslant0.8\,\mu\text{m}^{-1}$. However, the same result is obtained by fitting the slope between I and J with the average curve. In

addition, several recent studies (Mathis 1986; Clayton and Mathis 1988; Cardelli, Clayton, and Mathis 1988) have shown that for a large range of R values, the shape of observed extinction curves below $\lambda^{-1} \approx 0.9\,\mu\mathrm{m}^{-1}$ is essentially invariant. The IR extinction for the region $0.31\,\mu\mathrm{m}^{-1} \leqslant \lambda^{-1} \leqslant 0.54\,\mu\mathrm{m}^{-1}$ determined from IR H_2 molecular lines arising in the Orion molecular cloud (Davis, Larson, and Hofmann 1986) was fitted to the data in Fig. 3(b) and overplots the region corresponding to the two light circles in Fig. 3(b). We therefore find that the shape of the extinction curve for θ Ori longward of $\lambda \approx 5500$ Å is the same as the average interstellar curve.

Clearly, significant deviations in the shape of peculiar extinction compared to the average curve arise in the optical and are carried over into the UV. Thus, extinction-curve deviations from the norm in the optical, which can often appear insignificant when curves are normalized by $E(B-V)$, can have a profound effect on the appearance of the UV portion of the curve. Behavior similar to that seen in Fig. 3(b), although not as extreme, is exhibited by numerous lines of sight in the ρ Oph dark cloud (e.g., HD 147889; Whittet, van Breda, and Nandy 1973). The turnover of the optical extinction clearly leads to larger R values and a flatter linear background in the UV, which, if not taken into consideration, could lead to erroneous conclusions about the UV dust component(s) (see Sec. IV*c* below).

2) Ultraviolet

Fitzpatrick and Massa (1986, 1987) have been able to fit UV extinction curves as linear combinations of a Drude bump profile, a linear background, and a far-ultraviolet (FUV) curvature function. There are six parameters involved in the fit: the strength, central wavelength, and width of the bump, the slope and intercept of the linear background, and the strength of the FUV curvature. They examined a sample of 45 Galactic stars, which included θ^1 Ori C, θ^1 Ori D, NU Ori, and LP Ori. The sample sight lines were divided into three groups by type of environment. These were lines of sight associated with diffuse interstellar medium, dense clouds, and sites of recent early-type star formation. The Orion Nebula stars were placed in the latter group. Fitzpatrick and Massa find that:

(i) The slope and intercept of the linear background are well correlated for the whole sample.

(ii) The linear background parameters are not well correlated with any of the bump parameters or the FUV curvature.

(iii) The strength of the FUV curvature is correlated with the bump width.

(iv) The linear background and the bump width respond to changes in environment. The bump width tends to be broad for the dense cloud group and narrower for the diffuse and star-formation groups. The slope of the linear background is smaller for the dense and star-formation groups than for the diffuse group.

The lack of correlation between the linear background and the bump indicates that these features arise from separate grain populations. The very anomalous appearance of the Orion Nebula curves is due to the zero slope of the linear background toward these stars. However, Fitzpatrick and Massa (1987) find that the slope and intercept of the linear background in the Orion stars fit the same relationship as the other stars in their sample. Therefore, the lines of sight toward the Orion Nebula are not anomalous, they are just an extreme case of normal behavior.

The different slopes of the linear background can be understood in one of two ways (Fitzpatrick and Massa 1987). The slopes could be a family of extinction curves produced by an evolutionary process such as shocks. Alternatively, if there are two grain populations that produce different slopes, then mixing them in differing amounts along various lines of sight will produce different slopes. The two populations could be chosen such that one causes grey FUV extinction and the other causes extinction that is linear through the visual and the UV. Then most lines of sight with a mix of the two would have an intermediate slope, but extreme slopes would be seen along lines of sight where one population dominates. The line of sight toward HD 204827, which has a very steep slope, is an example of linear-extinction domination, and the Orion Nebula stars are an example of grey-extinction domination.

The slope of the linear background indicates that the Orion Nebula stars are an extreme case of the dense cloud group, but the narrowness of the bumps in this region is similar to that seen along diffuse lines of sight. One possible explanation of the bump-width variations is that small graphite grains form very thin amorphous carbon coatings. This does not significantly change the bump position but increases the bump width by about 10% (Hecht 1981). However, it should be noted that other explanations for the bump-width variations have been suggested (Hecht 1986; Fitzpatrick and Massa 1986). It seems somewhat contradictory that Orion Nebula extinction curves have characteristics in common with both dense-cloud and diffuse-medium stars. This behavior might be understood if the thin coatings were deposited on the bump grains inside the molecular cloud but were easily evaporated when the grains were exposed to the Trapezium environment before other grains had time to be significantly altered. This is discussed further in Sec. IV*c*.

b) The Orion Nebula Environment

Understanding the Orion Nebula dust is complicated by the probability that most of the known processes for grain growth, processing, and destruction may be occurring in close proximity to one another. The θ^1 Ori stars lie only a couple of tenths of a parsec in front of the molecular cloud from which they recently formed. The θ^1 and θ^2 Ori stars are the latest in a sequence of at least four episodes of star formation, each probably triggering the next, each delving deeper into the molecular cloud. Star formation in the region has been going on for about 12×10^6 yr, and the θ^1 and θ^2 Ori stars themselves may be as young as 5×10^5 yr (Abt 1979). The θ^1 and θ^2 Ori stars have each formed H II regions like blisters on the molecular cloud and they are density bounded so there is neutral material in front of these stars along the line of sight (Goudis 1982). The θ^2 Ori stars lie a few arcminutes southeast of the θ^1 Ori stars in an H II region disconnected from the θ^1 Ori (Trapezium) H II region (see Fig. 1 of Peimbert 1982). An ionization front lies between the two, indicating a tongue of neutral material. The extinction is slightly lower in the θ^2 Ori region, and the small amount of dust and CO emission indicates that it is somewhat foreground to the θ^1 Ori stars, which lie very close to the background molecular cloud.

Since the θ^1 Ori stars are the fourth in a sequence of star-formation episodes, each of which has penetrated deeper into the molecular cloud, the dust exposed in this episode

may have spent a considerable amount of time deep in the molecular cloud. The extreme youthfulness of the $\theta^{1,2}$ Ori cluster also allows the possibility that the dust surrounding it has been exposed for such a brief time that little processing of the grains has occurred. Infrared measurements have shown that the dust in and around the Trapezium is quite warm, from at least 250 K in the center of the Trapezium to about 70 K in the bar between the θ^1 and θ^2 H II regions (Goudis 1982). Churchwell *et al.* (1987) have observed as many as 29 ultracompact radio sources in the core of the Orion Nebula within the H II region. Some of these are nebular condensations which may be dense molecular globules or low-mass stars surrounded by protostellar accretion disks. In either case, these condensations are being ionized from the outside by UV radiation in the H II regions. Therefore, dust is being released inside the H II region that may still be molecular cloud dust protected in these condensations. Measured abundances in the H II region show almost exactly the same depletions as the line of sight toward ζ Oph (Pottasch 1985). If these depletions are attributed to condensation into dust grains, then 75% of C, N, and O atoms and almost all of Fe, Ca, and Al are locked up in dust (Spitzer 1978).

There is a cavity in the dust within about 3′ of the θ^1 Ori stars (Goudis 1982). Inside this cavity, the dust is depleted and the dust-to-gas ratio is lower than normal but increases with distance from the Trapezium (Mathis *et al.* 1981). Inside the H II region core, the strong UV radiation field creates a harsh environment for the grains. Radiation pressure will accelerate the dust grains and push them toward the edge of the region. The ionized gas may be strongly coupled to the grains and be dragged along with the dust (McCall 1981). Observations of molecular lines show evidence for low-velocity shocks associated with the ionization front of the H II region (Schloerb and Loren 1982). There are no high-velocity shocks present such as would be necessary to break up large grains (Seab 1987). It is possible that in the short lifetime of the θ Ori stars there have been no nearby supernovae. The rate of supernova explosions in an OB association is 1 per 10^5 to 2×10^6 yr (Cowie, Songaila, and York 1979). The supernova remnant forming Barnard's Loop is thought to be about $1\text{–}2\times10^6$ years old (Goudis 1982).

The presence of ongoing star formation, and a strong UV radiation field, suggest that dust cannot exist long in the Orion Nebula region without undergoing some evolution. An example of what evolution might occur can be seen in the dust in Cep OB3. Massa and Savage (1984) found a relationship between the slope of the linear-background extinction and the projected distance of a line of sight from the Cep OB3 molecular cloud. Close to the cloud, the linear background is flatter than normal. As the distance from the cloud increases, the slope of the linear background steepens and approaches the average Galactic value.

An example of the possible future of the Orion dust can be seen in the Trumpler 37 cluster. This is an H II region powered by a trapezium system which is eating into a complex of neutral clouds. The stars in this system are about 3×10^6 years old. Although this environment sounds similar to the Orion Nebula, this cluster contains HD 204827, mentioned above, which had the steepest UV linear-background extinction known in the Galaxy. UV extinction curves for about 15 members of this cluster have been calculated, and the linear background is generally steeper than the Galactic average throughout the cluster (Clayton and Fitzpatrick 1987). On the other hand, HD 204827 shows a wide bump more typical of dense cloud environments (Fitzpatrick and Massa 1986). The much greater age of this cluster implies that there has been time for processing of the grains, and Clayton and Fitzpatrick suggest a supernova shock as the processing agent.

c) Orion Dust: History and Evolution

Although they are extreme examples of deviation from normal dust extinction, the Orion curves show the same basic features as lines of sight elsewhere in the Galaxy. Therefore, the same grain constituents are probably present as elsewhere. For example, 9.7 μm emission is seen in the Orion Nebula, indicating the presence of silicate dust (Draine and Lee 1984). Also, although narrower than average, the presence of the UV 2175 Å bump indicates the presence of the standard bump carrier. Thus, it appears that a silicate population is responsible for the linear part of the optical and UV extinction while another population, perhaps amorphous graphite, is responsible for the bump (Tielens and Allamandola 1987). If the dust components are basically similar to other lines of sight, then what mechanism(s) are responsible for creating the current shape of the extinction seen toward $\theta^{1,2}$ Ori? Below, we discuss a possible evolutionary history of dust in the direction of the Orion Nebula.

1) Prestellar molecular cloud: Growth

It is a generally accepted notion that the shapes of the optical curves shown in Figs. 1 and 2 are characteristic of a shift of the particle-size distribution toward larger sizes, which is consistent with the observed larger R and $\lambda_{\max}$ (McCall 1981) values. Similar behavior is seen towards other lines of sight (e.g., HD 147889 in Ophiuchus; Whittet, van Breda, and Nandy 1973) where grain growth is indicated. For the portion of the curve $1.4\,\mu\text{m}^{-1}\leqslant\lambda^{-1}\leqslant3\,\mu\text{m}^{-1}$, it can be shown that an equally reasonable model fit to the observed extinction curve can be obtained by using monosize grains with $a_0=\langle a\rangle$, where $\langle a\rangle$ is the mean size for a discrete particle-size distribution where $n(a)\rightarrow0$ on either side of $\langle a\rangle$ (e.g., a log-normal function; Cardelli and Ackerman 1983). From this it can be shown that the optical extinction curves presented here represent a change in $\langle a\rangle$ of the order of 30%–60% with a corresponding change in R from the normal value of 3.1 to ≈5, which would be expected if changes in R arise in this portion of the extinction curve (Clayton and Mathis 1988; Cardelli, Clayton, and Mathis 1988).

If we assume that the change in grain size Δa is independent of size (Seab 1987), then it is, in principle, possible to create the above change in $\langle a\rangle$ via accretion from the gas phase if enough material were available. Evidence supporting this exists for lines of sight in dark clouds like Ophiuchus, where gas depletions are significantly higher than those seen in normal diffuse lines of sight (Cardelli 1984). Indeed, there is evidence that large depletions exist for the gas observed in the Orion Nebula (Pottasch 1985; Goudis 1982), with the values being on average between those found in diffuse lines of sight and the depletions seen toward Ophiuchus. However, the relative depletion of refractory elements seen in the Orion Nebula is larger than for C, N, and O, which appear similar to depletions seen in diffuse lines of sight. Thus, because $\langle a\rangle$ appears larger for grains in Orion than in Ophiuchus (as evidenced by the shape of the optical

extinction curves and the larger R values), it does not seem possible to explain the entire increase in $\langle a \rangle$ through accretion alone. (The relatively low depletion of volatile elements compared to the refractories would seem consistent with at least partial evaporation of mantles in the current environment (Mathis and Wallenhorst 1981)).

Another possible contribution to grain growth in cold, dark clouds is grain coagulation. Provided that the local gas turbulent velocity is not too large (Seab (1987) finds that large grains tend to shatter if $V_c \geqslant 0.1$ km s^{-1}), significant coagulation could occur over timescales of 10^4–10^5 yr if $n \geqslant 10^5$ cm^{-3} (McCall 1981), which is probably reasonable for the prestellar molecular cloud. An important consequence of coagulation is a decrease in the dust-to-gas ratio. Such a situation is observed in the Ophiuchus cloud (Jura 1980), and the smaller observed dust-to-gas ratio observed towards θ^1 Ori C seems to support this (Mathis *et al.* 1981).

Because there is ample observational support for both processes, it is likely that both accretion and coagulation were active in the cloud from which the Orion Nebula arose. However, based on current observed conditions, it would seem reasonable to assume that the effects of coagulation in the pre-nebula environment are the dominant cause of the large particles observed towards θ Ori (see below).

2) Current conditions: Destruction

Prior to the disruption of the region via the formation of $\theta^{1,2}$ Ori, it is quite possible that the dust extinction showed UV characteristics similar to dense lines of sight not associated with nebulosity in dark clouds like Ophiuchus (i.e., broad bump, steep FUV). Indeed, relative to the average interstellar extinction curve (Seaton 1979), there is evidence that lines of sight in Ophiuchus associated with nebulosity seem to exhibit, on average, narrower bumps and flatter FUV extinction similar to θ Ori. Other lines of sight associated with nebulosity that also show narrower than average bumps include Herschel 36 and stars in NGC 2244. Conversely, two extreme examples of lines of sight with the largest bump widths yet measured, HD 29647 and HD 62542, are associated with dark, dense clouds (Cardelli and Savage 1988). However, not all lines of sight associated with nebulosity exhibit narrow bumps such as the extremely broad bump observed toward ζ Oph. Thus, it appears that more than nebulosity contributes to the width of bumps (e.g., density and grain temperature). What will be particularly important is how closely the dust is associated with the nebula.

With $T_d \approx 100$–160 K (Goudis 1982) for dust near θ^1 Ori, sublimation of volatile mantles has certainly occurred (Martin 1978; Spitzer 1978), probably on very short timescales. For dust inside the H II region, thermal sputtering has also probably aided this process. According to the work of Hecht (1986), a possible explanation for bump-width variability is that sublimation of hydrogen and other impurities from the small carbon grains, responsible for the bump, can result in a selected narrowing of the bump. Evidence for the efficiency of these processes comes from the 2175 Å bump width for the θ^1 Ori stars, which at $\gamma \approx 0.86\ \mu\text{m}^{-1}$ (Fitzpatrick and Massa 1986) is significantly narrower than the average bump ($\gamma \approx 1.051\ \mu\text{m}^{-1}$; Fitzpatrick 1986). Support for this can be found in many lines of sight associated with nebulosity (see above) that exhibit narrower bumps, while lines of sight in dense environments not associated with nebulosity exhibit broader bumps (e.g., HD 147889). As pointed out above, although nebulosity is not necessarily the only effect, it would appear that the presence of strong radiation fields coupled with a moderate to low density environment can lead, on average, to narrower bumps. Conversely, even in the presence of nebulosity, high gas density may act to partially counter the effects of sublimation, as may be the case for the high-density environment seen toward ρ Oph (Snow and Jenkins 1980). Dust temperatures may also be selectively lower in such environments. For the Orion Nebula, it seems reasonable to assume that most or all of the mantles, particularly the volatile ones, have been removed. It is interesting to note that if this is strictly true, then the presence of larger than normal grains would seem to support the scenario that these larger grains have resulted from coagulation.

Seab (1987) has shown that shocks with $V_s \geqslant 100$ km s^{-1} are very effective at modifying grain-size distributions by preferentially destroying larger grains ($\geqslant 50\%$ for $a \geqslant 0.2\ \mu$m while only $\approx 3\%$ at $a \approx 0.01\ \mu$m), particularly silicates. However, such a process tends to increase the relative contribution of the bump and FUV extinction, which is not observed. Clearly, significant destruction of the larger grains is not indicated by the optical extinction. In addition, no gas motions greater than 30 km s^{-1} are observed (Wilson *et al.* 1959).

McCall (1981) has proposed that a reduction of the number of small grains would be possible through preferential evaporation and/or sputtering via stellar winds. He argues that such destruction could efficiently occur on timescales of $< 10^4$ yr, which he uses to explain the presence of larger grains as implied by the larger than normal values of $\lambda_{\max}$. While this seems reasonable for the direction to θ^1 Ori, it is not clear that it is equally applicable to the lines of sight to θ^2 Ori. If not, then it is difficult to understand why the θ^1 and θ^2 Ori extinction curves are nearly identical.

A final possible mechanism for modification of the dust is acceleration via radiation pressure. Though not strictly a destruction mechanism, size-dependent acceleration of grains can result in a change in the size-dependent column density $N(a)$. Nandy and Wickramasinghe (1971) conclude that grains with $a \geqslant 0.1\ \mu$m could be retained within the H II region for $t > 10^7$ yr, while grains with $a \leqslant 0.01\ \mu$m would be dispersed on a much smaller timescale. By including the effects of collisional and Coulombic drag forces, McCall (1981) has computed the relative separation expected for grains of different sizes in the direction of θ^1 Ori. He finds that at a distance of $r = 0.4$ pc, grains with $a \approx 0.1\ \mu$m and $0.4\ \mu$m will separate by $\Delta r = 0.01$ pc ($\Delta r/r \approx 0.025$) in 10^4 yr.

3) Extinction curves: Interpretation

From the above discussions, it seems to follow that the larger than normal grains giving rise to the optical extinction most likely have resulted primarily from coagulation in the prestellar molecular cloud. Most or all of the mantles have probably been removed in the time since the creation of the H II region. Radiation-induced thermal evaporation of small grains may also be occurring, the result of which will be to lower the effective column density of small grains relative to the large grains. Such an effect is desirable since the UV extinction seems to result from particles of the order of $a \leqslant 0.01\ \mu$m, and toward Orion it appears to be lower than normal. However, as pointed out above, it is difficult to understand how this process could operate equally efficiently toward both θ^1 and θ^2 Ori. Because it produces the same effect, differential radiation pressure could produce the desired reduction in the small-particle column density. For small grains characterized by $a = 0.01\ \mu$m, values of $\Delta r/$

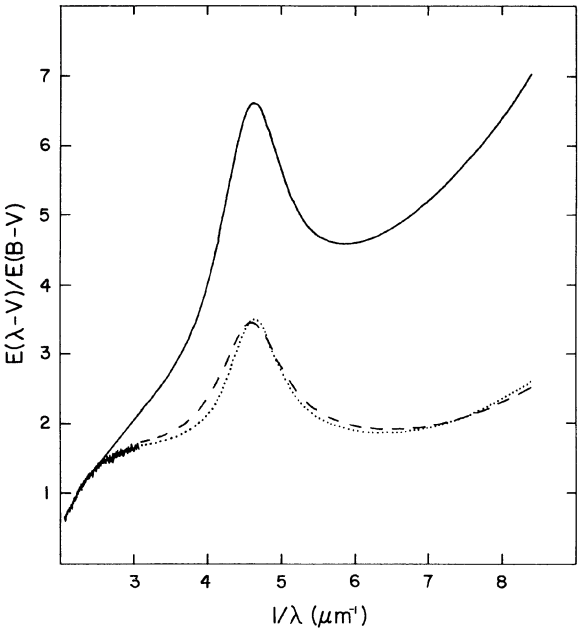

FIG. 4. The solid curve represents the normalized average interstellar extinction curve, while the dotted curve represents the average curve for θ Ori. The dashed curve results from the combination of the computed UV linear background for θ Ori (Fitzpatrick and Massa 1986) and the bump and FUV components derived from the Seaton curve (Fitzpatrick 1986) divided by a factor of about 1.8. Excluding the narrower appearance of the θ Ori bump, the agreement is quite good, which implies that UV extinction toward the Orion Nebula can be viewed simply as an increase in the size of the optical grain component and a reduction in the column density of otherwise normal UV grain components.

$r \geqslant 0.2$ could be achieved in 10^4 yr, which translates at $r = 0.4$ pc to a reduction in the effective small-particle column density of $\geqslant 36\%$.

Figure 4 represents an attempt to show how the effects of the above processes might produce curves like the ones seen toward θ Ori. The solid and dotted curves represent the normalized average extinction curve of Seaton (1979) and the mean θ Ori curve. Using the three-component approach for describing UV extinction curves (see Sec. IV*a*), the dashed curve was created by adding about 50%–55% of the strength of the bump and FUV components of the Seaton curve (Fitzpatrick 1986) to the UV linear background derived for the θ Ori curve (Fitzpatrick and Massa 1986). Thus, if the initial bump and FUV strengths per unit $E(B - V)$ appropriate for the Orion Nebula are assumed to be the same as those appropriate for the average interstellar curve, then a 50%–55% reduction in the column density of these (normal) grains will reproduce the proper amount of normalized UV extinction. Assuming we initially started with grains characteristic of a Seaton-type curve and do not change the UV grain components, exactly how much of a reduction has actually occurred in the small-particle column density will depend on how the magnitude of A_λ changed for the optical grains in the molecular cloud. For example, keeping the total grain number fixed and growing all optical grains will result in a net increase in A_λ everywhere. Conversely, removing small optical grains without effectively changing the extinction per (large) grain will result in a net decrease in A_λ in the near-UV and UV. Assuming the net absolute contribution of the bump and FUV remains fixed in both cases, the apparent strength of both components in a normalized curve will be different for the two cases. Taking this into account, the probable range in the reduction of the column density of bump and FUV grains is of the order of 30%–70%.

In reality, a combination of both evaporation and evacuation of small grains in the inner nebular region has probably occurred and so reduction of the effective column density of the small UV grain components of 30%–70% is not unreasonable. The beauty of the above results is that the drastic abnormalities in the extinction curves observed toward the Orion Nebula can be plausibly explained in a relatively simple way. In other words, with the exception of the growth of optical grains, the observed abnormalities in the extinction are mostly due to the peculiarities of the environment and *not* the grains. It will be interesting to apply these results to other peculiar lines of sight (e.g., Ophiuchus and R CrA) to see if these results hold in general.

V. SUMMARY

New high-quality optical extinction curves have been calculated for five of the θ Ori stars. These curves fit together very well with the UV curves of Bohlin and Savage (1981), strongly confirming the reality of the early turnover of the linear portion of the extinction curve resulting in flat UV extinction. The turnover occurs as early as 5000 Å and is related to the large calculated values of R for these stars. Therefore, R is an indicator of flatter than normal UV extinction.

The dust producing the average θ Ori extinction curve could plausibly be composed of:

(i) A population of silicate grains, providing the optical and UV linear-background extinction which turns over and becomes flat at optical wavelengths. These grains resided, until recently (5×10^5 yr), inside the molecular cloud. They have grown larger than normal through coagulation and accretion.

(ii) A population of small carbon grains, providing the bump extinction, which is narrower than bumps seen in dense quiescent regions. They have lost their volatile mantles through evaporation from the intense local radiation field.

(iii) Radiation pressure in the Orion Nebula separates small and large grains by a significant amount, reducing the contribution of the small grains to the extinction curve. This has the effect of weakening the bump and FUV extinction and increasing the effect of the larger than normal silicate extinction. This effect may also be enhanced by selected evaporation/sputtering of small grains.

REFERENCES

Abt, H. A. (1979). Astrophys. J. **230**, 485.
Anderson, C. M. (1970). Astrophys. J. **160**, 507.
Baade,W., and Minkowski, R. (1937). Astrophys. J. **86**, 123.
Bohlin, R. C., and Savage, B. D. (1981). Astrophys. J. **249**, 109.
Breger, M., Gehrz, R. D., and Hackwell, J. A. (1981). Astrophys. J. **248**, 963.
Cardelli, J. A. (1984). Astron. J. **89**, 1825.
Cardelli, J. A., and Ackerman, T. P. (1983). Publ. Astron. Soc. Pac. **95**, 451.
Cardelli, J. A., Clayton, G. C., and Mathis, J. S. (1988). In preparation.
Cardelli, J. A., and Savage, B. D. (1988). Astrophys. J. (in press).
Carruthers, G. R. (1969). Astrophys. J. Lett. **157**, L111.

Churchwell, E., Felli, M., Wood, D. O. S., and Massi, M. (1987). Astrophys. J. **321**, 516.
Clayton, G. C., and Fitzpatrick, E. L. (1987). Astron. J. **93**, 157.
Clayton, G. C., and Mathis, J. S. (1988). Astrophys. J. (in press).
Conti, P. S., and Aschuler, W. R. (1971). Astrophys. J. **170**, 325.
Cousins, A. W. J., Lake, J., and Stoy, R. H. (1966). R. Obs. Bull. No. 121.
Cowie, L. L., Songaila, A., and York, D. G. (1979). Astrophys. J. **230**, 469.
Davis, D. S., Larson, H. P., and Hofmann, R. (1986). Astrophys. J. **304**, 481.
Draine, B. T., and Lee, H. M. (1984). Astrophys. J. **285**, 89.
FitzGerald, M. P. (1970). Astron. Astrophys. **4**, 234.
Fitzpatrick, E. L. (1986). Astron. J. **92**, 1068.
Fitzpatrick, E. L., and Savage, B. D. (1984). Astrophys. J. **279**, 578.
Fitzpatrick, E. L., and Massa, D. (1986). Astrophys. J. **307**, 286.
Fitzpatrick, E. L., and Massa, D. (1987). Astrophys. J. (submitted).
Garrison, R. F. (1967). Astrophys. J. **147**, 1003.
Goudis, C. (1982). *The Orion Complex: A Case Study of Interstellar Matter* (Reidel, Dordrecht).
Hecht, J. H. (1981). Astrophys. J. **246**, 794.
Hecht, J. H. (1986). Astrophys. J. **305**, 817.
Jacoby, G. H., Hunter, D. A., and Christian, C. A. (1984). Astrophys. J. Suppl. **56**, 257.
Johnson, H. L. (1958). Lowell Obs. Bull. **4**, 37.
Johnson, H. L. (1966). Commun. Lunar Planet. Obs. **4**, 99.
Johnson, H. L. (1967). Astrophys. J. Lett. **150**, L39.
Johnson, H. L. (1968). In *Nebulae and Interstellar Matter*, edited by B. A. Middlehurst and L. H. Aller (University of Chicago, Chicago).
Jura, M. (1980). Astrophys. J. **253**, 63.
Lee, T. A. (1968). Astrophys. J. **152**, 913.
Lesh, J. R. (1968). Astrophys. J. Suppl. **17**, 371.
Martin, P. G. (1978). *Cosmic Dust* (Clarendon, Oxford).
Massa, D., and Fitzpatrick, E. L. (1986). Astrophys. J. Suppl. **60**, 305.
Massa, D., and Savage, B. D. (1984). Astrophys. J. **279**, 310.
Massa, D., Savage, B. D., and Fitzpatrick, E. L. (1983). Astrophys. J. **266**, 662.
Mathis, J. S. (1986). Astrophys. J. **308**, 281.
Mathis, J. S., Perinotto, M., Patriarchi, P., and Schiffer III, F. H. (1981). Astrophys. J. **249**, 99.
Mathis, J. S., and Wallenhorst, S. G. (1981). Astrophys. J. **244**, 483.
McCall, M. L. (1981). Mon. Not. R. Astron. Soc. **194**, 485.
Nandy, K., and Wickramasinghe, N. C. (1971). Mon. Not. R. Astron. Soc. **154**, 255.
Osterbrock, D. W. (1974). *Astrophysics of Gaseous Nebulae* (Freeman, San Francisco).
Panek, R. J. (1983). Astrophys. J. **270**, 169.
Peimbert, M. (1982). Ann. N. Y. Acad. Sci. **395**, 24.
Penston, M. V., Hunter, J. K., and O'Neill, A. (1975). Mon. Not. R. Astron. Soc. **171**, 219.
Pottasch, S. R. (1985). In *The Milky Way Galaxy*, IAU Symposium No. 106, edited by H. van Woerden, R. J. Allen, and W. B. Burton (Reidel, Dordrecht), p. 580.
Rieke, G. H., and Lebofsky, M. J. (1985). Astrophys. J. **288**, 618.
Schiffer III, F. H., and Mathis, J. S. (1974). Astrophys. J. **194**, 597.
Schloerb, F. P., and Loren, R. B. (1982). Ann. N. Y. Acad. Sci. **395**, 32.
Seab, C. G. (1987). In *Interstellar Processes*, edited by D. J. Hollenbach and H. A. Thronson (Reidel, Dordrecht), p. 491.
Seaton, M. J. (1979). Mon. Not. R. Astron. Soc. **187**, 73p.
Snow, T. P., and Jenkins, E. B. (1980). Astrophys. J. **241**, 161.
Spitzer, L. (1978). *Physical Processes in the Interstellar Medium* (Wiley, New York), p. 4.
Stebbins, J., and Huffer, C. M. (1934). Publ. Washburn Obs. **15**, 215.
Tielens, A. C. G. M., and Allamandola, L. J. (1987). In *Interstellar Processes*, edited by D. J. Hollenbach and H. A. Thronson (Reidel, Dordrecht), p. 397.
Underhill, A. B. (1966). *The Early Type Stars* (Reidel, Dordrecht), p. 50.
Walborn, N. R. (1971). Astrophys. J. Suppl. **23**, 257.
Whitford, A. E. (1958). Astron. J. **63**, 201.
Whittet, D. C. B., van Breda, I. G., and Nandy, K. (1973). Nature Phys. Sci. **243**, 21.
Wilson, O. C., Münch, G., Flather, E. M., and Coffeen, M. F. (1959). Astrophys. J. Suppl. **4**, 199.
Wu, C. -C., Gilra, D. P., and van Duinen, R. J. (1980). Astrophys. J. **241**, 173.